Journal of Southeast University (English Edition) Vol. 36, No. 2, pp. 227 - 233 June 2020 ISSN 1003—7985

Influence evaluation of titania nanotube surface morphology on the performance of bioelectrochemical systems

Zhang Tian[1] Long Xizi[1] Cao Xian[2] Li Xianning[1]

([1]School of Energy and Environment, Southeast University, Nanjing 210096, China)

([2]Department of Civil and Environmental Engineering, Tohoku University, Sendai 980-8579, Japan)

Abstract: In order to investigate the effect of the surface morphology and resistance of the TiO_2 semiconductor on current output, TiO_2 nanotube array bio-anodes (TNA) are synthesized at different electrolyte temperatures, thereby changing the length and surface roughness of the nanotubes. When the anodizing temperature is increased from 30 to 75 ℃, the length of the nanotubes increases from 1.459 to 4.183 μm, which hinders the transfer of extracellular electrons to the electrodes. On the other hand, the surface roughness of TNA is significantly improved at higher temperatures, which is conducive to electron transfer. Therefore, samples processed at 45 ℃ have the best current output performance. Compared with the treatment at 30 ℃ under anodization, samples processed at 45 ℃ can balance the resistance and roughness and have a higher electron transfer rate; the current output density of which is increased by 1.5 times, and the decolorization rate is increased by 0.8 times. Therefore, proper TNA surface morphology can improve the current output and the potential of wastewater treatment.

Key words: bioelectrochemical system; titania nanotube arrays; anodization; current generation; surface morphology

DOI: 10.3969/j.issn.1003 - 7985.2020.02.014

Microbial bioelectrochemical systems (BESs) are microbial engineering systems which utilize microorganisms as living catalysts to interconvert electrical and chemical energy[1]. The representative BES can be used in microbial fuel cells (MFCs). The microbial fuel cell is a newly developed technology for simultaneous power generation and wastewater treatment[2], and it is a typical microbial bioelectrochemical system. In MFCs, electroactive bacteria (EAB) on the electrode catalyzes the oxidation of organics to electrons via complex extracellular electron transfer (EET), which is regarded as the main limitation of commercial applications[3]. Efforts have been made to improve EET by identifying bacteria that generate more power, designing cells that better transmit power, and promoting biofilm accumulation on modified electrodes[4]. Compared with carbon materials (e.g., graphite), metal electrodes have a higher conductivity and greater mechanical strength. However, apart from noble metals, most metals corrode easily and have poor biocompatibility[5].

Titanium (Ti) is corrosion-resistant and biocompatible and, thus, is widely used in biosensors, medicine delivery and implants. However, in order to decrease costs and improve the surface binding of cells, different titania nanostructures have been synthesized, including nanotubes, nano-wires, nano-rods, and nano-nets[6-7]. Electrochemical anodization can be used to alter the highly ordered surface morphology of titania nanotube arrays (TNAs) by controlling parameters such as the electrolytes, voltage, and process time[8]. A wide range of lengths (1 to 200 μm) and pore diameters (20 to 150 nm) have been produced for different applications[9]. Moreover, the application of different TNAs on photocatalysis and wastewater treatment in MFCs has been widely studied in recent decades[10-11].

Few studies have detailed bacterial cell-TNA interactions. Feng et al.[7] first investigated the current output of TNA anodes. Compared with bare Ti plates, a 190-fold higher current density of (12.7 ± 0.7) A/m^2 was observed in TNA, which improved the accumulation of EAB on the nanotube structure. Furthermore, Anitha et al.[12] quantified the influence of nanotube diameter on the growth of biofilms. A 20-nm diameter corresponding to a 90% increase in the surface area (compared with 140 nm) resulted in better adhesion of EAB. A study of the crystallinity of TNA electrodes examined heating treatments in hydrogen, methane, and nitrogen atmospheres[13]. Higher crystallinity in a reducing hydrogen atmosphere markedly improved biofilm formation on the anode. However, titanium dioxide has a huge band gap of 3.2 eV[14], which results in the poor conductivity of nanotubes merely comprised of titania. In fact, multimeter detection revealed that the TNAs in this study exhibi-

Received 2019-12-14, **Revised** 2020-03-08.

Biographies: Zhang Tian (1994—), female, graduate; Li Xianning (corresponding author), male, doctor, professor, lxnseu@163.com.

Foundation items: The National Major Science and Technology Project (No. 2017ZX07202004-005), the Natural Science Foundation of Jiangsu Province (No. BK20171351), the Japan Society for the Promotion of Science (No. P 19056), the National Natural Science Foundation of China (No. 51828801), the Fundamental Research Funds for the Central Universities (No. 2242016K41042).

Citation: Zhang Tian, Long Xizi, Cao Xian, et al. Influence evaluation of titania nanotube surface morphology on the performance of bioelectrochemical systems[J]. Journal of Southeast University (English Edition), 2020, 36(2): 227 - 233. DOI: 10.3969/j.issn.1003 - 7985.2020.02.014.

ted a resistance of 3×10^4 Ω. Although the mechanism of the conduction of a bioanode is not clear, some research showed that a thin oxide layer at the bottom of nanotube pores and voids allows EET to occur. Therefore, the thicker TNA can increase resistance and affect the flow of the EET process. To the best of our knowledge, few reports have discussed the influence of tube length and surface morphology.

This study evaluates the power generation of TNA electrodes with different tube lengths and roughness. The length and roughness of the TNA are manipulated by electrochemical anodization at different temperatures. Moreover, the reduction kinetics of an azo dye is established to evaluate the EET capacity of the TNA anodes. Finally, a possible mechanism is considered by discussing the correlation among power generation, pipe diameter, and microbial community.

1 Materials and Methods

1.1 Electrochemical anodization for the synthesis of TNAs

TNAs of different lengths were synthesized according to previously reported methods. Briefly, a Ti plate with an area of 4 cm^2 was first cleaned in acetone, ethanol, and deionized water for 15 min, respectively. After drying, electrochemical anodization was performed for 5 h by loading a voltage of 30 V between the Ti plate and a graphite counter electrode. The electrolytes (1.092 g NaF, 160 mL ethylene glycol, and 40 mL distilled water) were heated to 30 ℃ (A1), 45 ℃ (A2), 55 ℃ (A3), 65 ℃ (A4), or 75 ℃ (A5) during synthesis. After anodization, the samples were washed by deionized water and dried with nitrogen. Then, the electrode was annealed in air at 450 ℃ for 2 h in a muffle furnace (SXL; Shanghai Jinghong, Shanghai, China).

1.2 MFC construction and operation

A double-chamber reactor (175 mL) divided by a cation-exchange membrane (CMI7000; Membrane International, Glen Rock, NJ, USA) was used. The anode chamber was inoculated with 15 mL of effluent from the cathode of a continuous-flow denitrification MFC. The anolyte comprised of 0.1 g/L active brilliant red X-3B (ABRX3), 0.5 g/L NaAC, 0.025 g/L NH_4Cl, 1.66 g/L $NaH_2PO_4 \cdot 2H_2O$, 5.16 g/L $Na_2HPO_4 \cdot 12H_2O$, and trace elements[10]. Before batch experiments, the anolyte was pre-deoxygenated via nitrogen bubbling for 30 min. The anolyte was stirred magnetically and replenished every 3 d when the current dropped. A 100 Ω external resistor was loaded between two electrodes during the whole experiment process.

1.3 Characterization of TNA electrodes

A field emission scanning electron microscope (FESEM) operating at 10 kV (Nova NanoSEM 450; FEI, Hillsboro, OR, USA) was used to characterize the morphology of the top and tube sides of the TNAs.

1.4 Analysis

The current in the MFC was recorded every 30 s[11]. Cyclic voltammetry (CV) was conducted in the presence of NaAC in the anolyte under the turnover condition and in absence of organics under no turnover condition at different scan rates. Ag/AgCl electrode was the reference eletrode. Electrochemical impedance spectroscopy (EIS) was used (100 kHz to 0.01 Hz) to measure the resistance of the material[11].

The electrontransfer number is calculated by a simple model as follows:

$$J = \frac{J_{\text{limit}}}{1 + \exp(nF(E^0 - E)/RT)} \tag{1}$$

where J and J_{limit} are the current and limited current output (mA), respectively, in the presence of organic material in the anolyte, which is referred to as the turnover condition. E^0 is the half-peak potential of the current profile; n is the electrons; F is the Faradic constant; and F = 96 485 C/mol. R is the ideal gas constant, R = 8.314 J/(mol · K), and T is the temperature, K.

To quantify the rate of ABRX3 degradation, a first-order kinetics model is applied as follows:

$$\frac{dc}{dt} = -kc \tag{2}$$

where c is the concentration of ABRX3 in water at time t, mg/L; and k is the first-order kinetic constant. Each sample was collected with a syringe and filtered through a 0.45-μm filter before analysis. The absorbance variation at the catholyte was measured using UV-Vis spectrophotometry (UV9100; Labtech International Ltd, East Sussex, UK) from 200 to 700 nm. The microbial community structures of A1 to A5 were examined using 16s rRNA pyrosequencing.

2 Results and Discussion

As shown in Fig. 1, the lengths of the TNAs A1 to A5 are 1.459, 2.322, 3.043, 3.430, and 4.183 μm, respectively. The growth of TNAs increased significantly with the anodization temperature. The etching effect of F^- on titanium dioxide was enhanced at higher temperatures, increasing the lengths of the nanotubes. According to previous research, electrochemical corrosion and the growth of TNAs proceed simultaneously in organic solvents, such as ethylene glycol and methanol[15]. The nanotubes can reach hundreds of micrometers in length. However, as a high volume ratio of water was used in this experiment, the chemical dissolution rate of the TNAs in aqueous solution was very fast, resulting in shorter nanotubes (< 4.5 μm). Apart from altering the

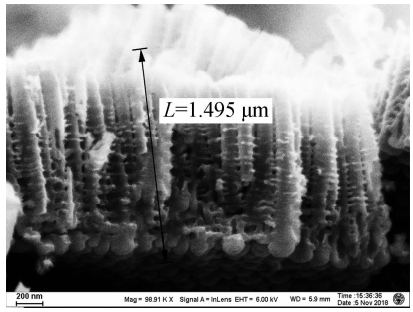

(a)

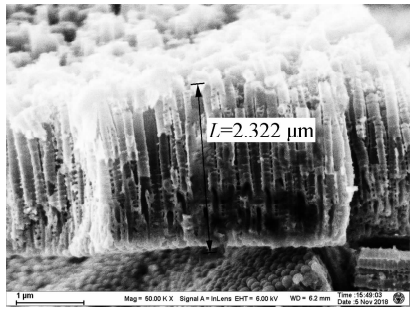

(b)

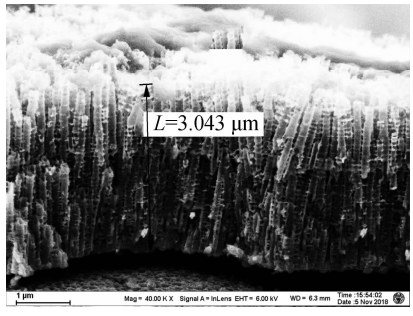

(c)

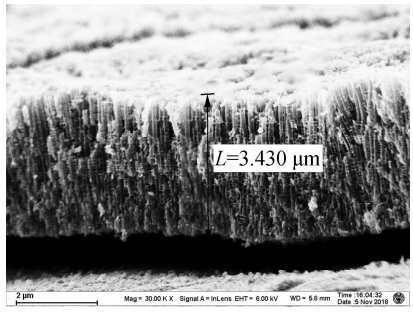

(d)

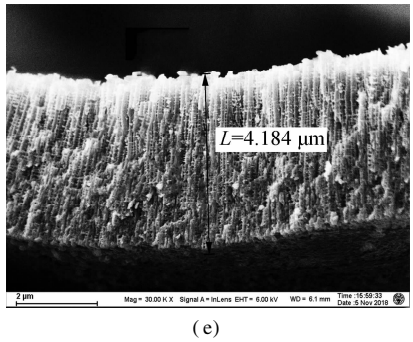

(e)

Fig. 1 Scanning electron microscopy images of the titania nanotube arrays. (a) A1; (b) A2; (c) A3; (d) A4; (e) A5

length, little effect on the surface pore size of the TNAs was observed[16]. Bulges grew along the pipe. Previous studies have shown that the distance between the bulges on the tube wall was the same, indicating that the formation of the bulges on the tube wall was related to the current oscillation[17].

Fig. 2(a) shows the current output of the anodes. The maximum current densities observed in A2 (0.625 mA/cm^2), A5 (0.5 mA/cm^2), A4 (0.45 mA/cm^2), A3 (0.4 mA/cm^2), and A1 (0.25 mA/cm^2) were recorded after 20 d of acclimation. Although there were similar cycles of current increase and decrease between the replenishment of the anolyte, the start-up of A1 was much slower (12 d) than that of the others. This delayed current increase reflected the lower accumulation of EAB on the surface of A1, whereas electrodes made at higher anodization temperatures accumulated more EAB and generated more current. The kinetics of EET were evaluated by CV spectroscopy in Fig. 2(b). By Eq. (1), the apparent electron transfer was calculated. In this study, the values of A2 and A1 were 0.213 and 0.107, respectively. An S-shaped CV curve usually represents the rate of oxidation of organic matter in cells by EAB[18]. More electrons in A2 resulted in better electrode performance[10]. Due to the band gap of titanium dioxide being 3.2 eV, a huge surface resistance of approximately 10^{20} ($\Omega \cdot m$)$^{-1}$ was observed[17]. According to Fig. 1, A1 TNA (1.459 μm) was shorter than A2 TNA (2.322 μm); thus, A1 exhibited a lower resistance. However, the current generated by A1 was still 1.5 times lower than that generated by A2. In comparison, although the tube length of A5 was 4 times as long as A1, A5 still generated more current. Accordingly,

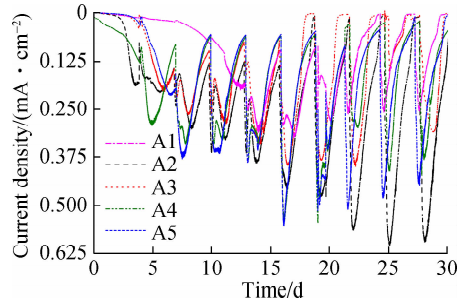

(a)

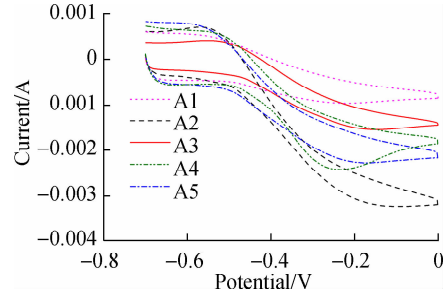

(b)

Fig. 2 Current output characteristics. (a) Time profile of the current outputs; (b) Results of turnover cyclic voltammetry spectroscopy

the surface morphology of TNAs was studied to understand the reason for these differences.

Fig. 3 shows the surface morphology of the TNAs. The pore size of the nanotubes did not change and was approximately 200 nm. The three-dimensional reconstruction of the SEM images shows that the surface roughness is improved greatly by changing the anodization temperature. Greater surface roughness is more suitable for microbial attachment, which can significantly increase the accumulation of EAB and the electricity generated[19-20].

The electrochemical characteristics of the TNAs are further evaluated (see Fig. 4). As the extracellular electron transfer (EET) by EAB is mainly realized by the outer membrane heme proteins/protein flavin complex, the surface proteins involved in electron transfer can be studied semi-quantitatively using non-turnover CV spectroscopy. As shown in Fig. 4(a), redox pairs are observed between −0.44 and −0.35 V (vs. Ag/AgCl), which typically appears in a mixed culture with Geobacter biofilms[21]. Surprisingly, a negative shift in the oxidation peaks from A1 (−0.41 V) to A5 (−0.48 V) was observed as the roughness increased. The semi-quinone complex formed by binding flavin and the outer membrane cytochrome resulted in more negative values[22-23]. This free radical changes the process of the 2-electron transfer into a single-electron transfer, which significantly accelerates extracellular electron transfer and increases current. In this experiment, the rougher interface locked more secreted

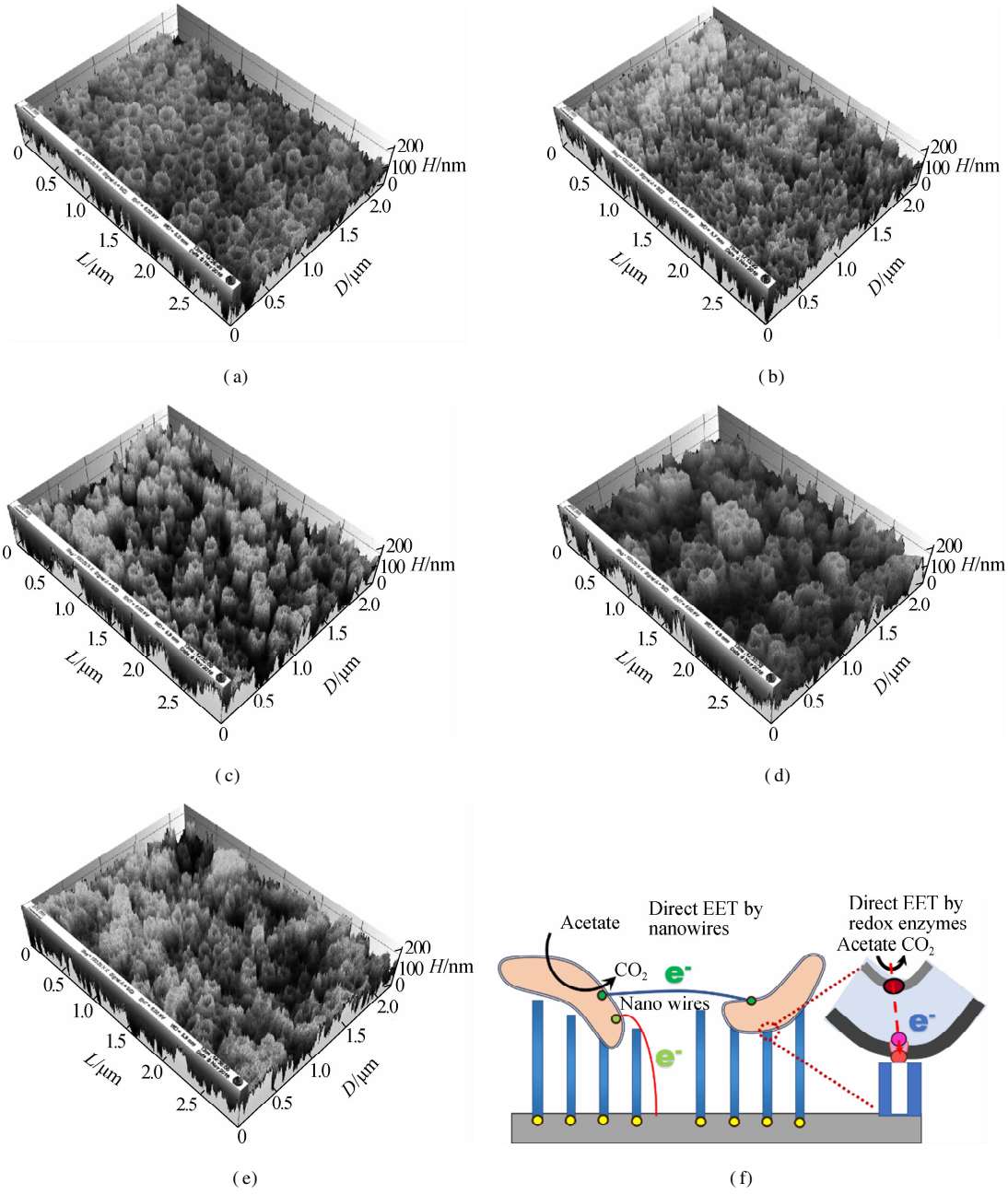

Fig. 3 SEM images of the top surface of the TNAs and a schematic of bacteria attaching to a TNA by EET. (a) A1; (b) A2: (c) A3; (d) A4; (e) A5; (f) A schematic of bacteria attaching to a TNA by EET

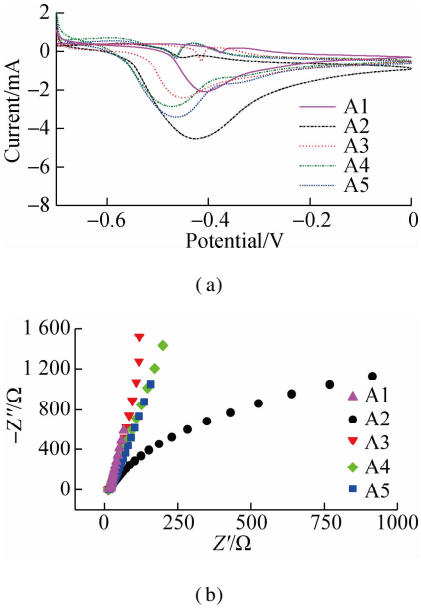

Fig. 4 Electrochemical analysis of the anode. (a) Results of non-turnover CV spectroscopy; (b) Results of electrochemical impedance spectroscopy of different anodes

flavin as a result of stirring, which contributed to a 70% increase in the current[22,24]. EIS was used to determine the resistance of the anodes. As shown in Fig. 4(b), the small arc in the Nyquist plot of A2 indicates its lower interface impedance. The diffusion and electron transfer resistances of A2 are 3,451 and 17.05 Ω, respectively, which are much lower than those of A1 (8.26×10^8 and 118.6 Ω, respectively). The lower resistance of A2 electrons contributes to the EET at the interface. Although the lower roughness of A2 hampers the enrichment of microorganisms compared with A3 to A5, the nanotubes in A2 are significantly shorter with a lower resistance, which might have contributed to the current output in this experiment. Notably, the highest current output of A2 might be caused by better balance between nanotube length and interface roughness.

Fig. 5(a) shows the ABRX3 decolorization during the batch periods. The highest removal ratio of 80% is obtained with A2 electrode, whereas the removal ratio of A1 is only approximately 59%. The removal constants are obtained by fitting the first-order kinetic model to the data (see Fig. 5(b)). The removal rate constant of A2 ($-0.009\ 71\ h^{-1}$) is 1.8 times that of A1 ($-0.005\ 46\ h^{-1}$). Although the application of azo dyes in MFCs has been studied in recent decades, researchers confirmed only recently that the outer membrane heme proteins of EAB reduce the azo bond[25–26]. As the azo dye methyl orange cannot penetrate the outer membrane of Geobacter, decolorization was achieved solely by the direct electron supply from the proteins OmcC, OmcE, and OmcB located on the outer membrane[26]. In this experiment, the higher current output from the A2 anode implied better accumulation of EAB at the interface where the azo bond was reduced. The first-order kinetic constants are analyzed using the peak current (see Fig. 4(a)). The linear correlation ($R^2 = 0.955$) between the peak current and removal rate constants confirmed that EAB played a role in azo dye removal. In general, A2 has better potential as the electrode, which can be used for wastewater treatment.

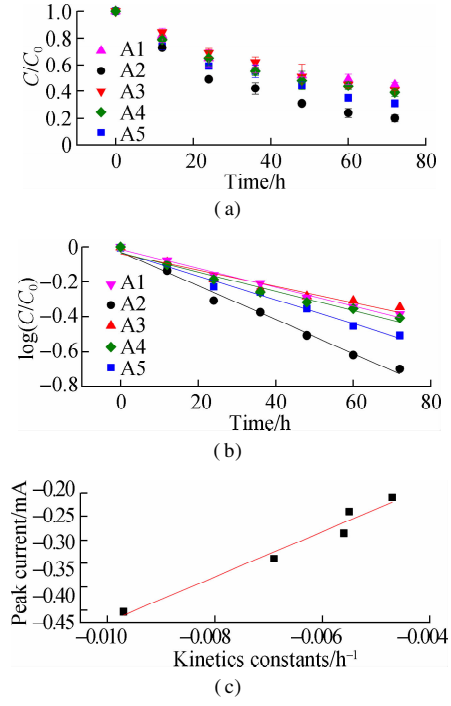

Fig. 5 Active brilliant red X-3B (ABRX3) degradation with different anodes. (a) ABRX3 decolorization over 72 h; (b) First-order kinetic constants fitted to represent decolorization at each anode; (c) Correlation between kinetics contents and peak current

Fig. 6(a) shows the microbial community structure of each TNA at the genus level. All anodes selectively accumulate the anode respiration bacteria Geobacter. The relative abundance of Geobacter in A1 to A5 are 0.655, 0.724, 0.725, 0.604 and 0.803, which is different and can significantly affect the current output[27]. The spearman correlation analysis of the microorganisms, current, and roughness showed that higher current and roughness corresponded to a greater abundance of Geobacter (see Fig. 6(b)). Therefore, the rough surface is conducive to the enrichment of electricity-producing microorganisms. It is noted that the relative abundance of A2 is slightly lower than that of A5, whereas its current output is higher than that of A5. These contrasting results indicate that the effect of surface roughness can be offset by a smaller resistance with shorter tubes.

3 Conclusions

1) TNA semi-conductor MFC anodes were prepared via anodization at temperatures ranging from 30 to 75 ℃. The surface morphology of TNA and the performance of the bioelectrochemical system are influenced by

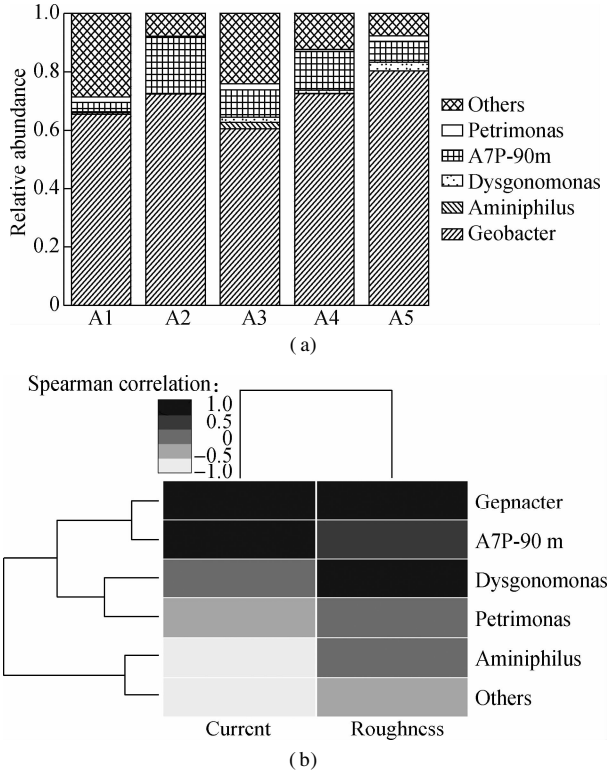

Fig. 6 Analysis of anode microbial community and correlation analysis of environmental factors of different anodes. (a) Microbial community structure of each anode classified at the genus level; (b) Spearman correlations between the microbial community, current and roughness

the anodization temperatures.

2) A four-fold increase in nanotube length was accompanied by increased roughness on the top interfaces of the TNAs. The stable current output and the azo dye decolorization rate of A2 were 2.5 and 1.8 times that of A1, respectively.

3) These features arose from the lower resistance of the relatively shorter tubes and the better attachment of EAB to the rough electrode surface.

References

[1] Liu S T, Feng X J, Li X N. Bioelectrochemical approach for control of methane emission from wetlands[J]. *Bioresource Technology*, 2017, **241**: 812 − 820.

[2] Logan B E, Hamelers B, Rozendal R, et al. Microbial fuel cells: Methodology and technology[J]. *Environmental Science & Technology*, 2006, **40**(17): 5181 − 5192.

[3] Rinaldi A, Mecheri B, Garavaglia V, et al. Engineering materials and biology to boost performance of microbial fuel cells: A critical review[J]. *Energy and Environmental Science*, 2008, **1**(4): 417 − 429. DOI: 10.1039/B806498A.

[4] Liang Y X, Feng H J, Shen D S, et al. Enhancement of anodic biofilm formation and current output in microbial fuel cells by composite modification of stainless steel electrodes[J]. *Journal of Power Sources*, 2017, **342**: 98 − 104. DOI: 10.1016/j.jpowsour.2016.12.020.

[5] Zheng X, Su Y L, Chen Y G, et al. Zinc oxide nanoparticles cause inhibition of microbial denitrification by affecting transcriptional regulation and enzyme activity[J]. *Environmental Science & Technology*, 2014, **48**(23): 13800 − 13807. DOI: 10.1021/es504251v.

[6] Yin T, Li H, Su L, et al. The catalytic effect of TiO_2 nanosheets on extracellular electron transfer of Shewanella loihica PV-4[J]. *Physical Chemistry Chemical Physics*, 2016, **18**(43): 29871 − 29878. DOI: 10.1039/c6cp04509j.

[7] Feng H J, Liang Y X, Guo K, et al. TiO_2 nanotube arrays modified titanium: A stable, scalable, and cost-effective bioanode for microbial fuel cells[J]. *Environmental Science & Technology Letters*, 2016, **3**(12): 420 − 424. DOI: 10.1021/acs.estlett.6b00410.

[8] Reyes-Gil K R, Robinson D B. WO_3-enhanced TiO_2 nanotube photoanodes for solar water splitting with simultaneous wastewater treatment[J]. *ACS Applied Materials & Interfaces*, 2013, **5**(23): 12400 − 12410. DOI: 10.1021/am403369p.

[9] Weon S, Choi W. TiO_2 nanotubes with open channels as deactivation-resistant photocatalyst for the degradation of volatile organic compounds[J]. *Environmental Science & Technology*, 2016, **50**(5): 2556 − 2563. DOI: 10.1021/acs.est.5b05418.

[10] Long X Z, Wang H, Wang C Q, et al. Enhancement of azo dye degradation and power generation in a photoelectrocatalytic microbial fuel cell by simple cathodic reduction on titania nanotube arrays electrode[J]. *Journal of Power Sources*, 2019, **415**: 145 − 153. DOI: 10.1016/j.jpowsour.2019.01.069.

[11] Long X Z, Pan Q R, Wang C Q, et al. Microbial fuel cell-photoelectrocatalytic cell combined system for the removal of azo dye wastewater[J]. *Bioresource Technology*, 2017, **244**: 182 − 191. DOI: 10.1016/j.biortech.2017.07.088.

[12] Anitha V C, Lee J H, Lee J, et al. Biofilm formation on a TiO_2 nanotube with controlled pore diameter and surface wettability[J]. *Nanotechnology*, 2015, **26**(6): 065102. DOI: 10.1088/0957 − 4484/26/6/065102.

[13] Huang L J, Zhang X Q, Shen D S, et al. Effect of heat-treatment atmosphere on the current generation of TiO_2 nanotube array electrodes in microbial fuel cells[J]. *Electrochimica Acta*, 2017, **257**: 203 − 209. DOI: 10.1016/j.electacta.2017.10.068.

[14] Mo S D, Ching W Y. Electronic and optical properties of three phases of titanium dioxide: Rutile, anatase, and brookite[J]. *Physical Review B*, 1995, **51**(19): 13023 − 13032. DOI: 10.1103/physrevb.51.13023.

[15] Macak J M, Tsuchiya H, Schmuki P. High-aspect-ratio TiO_2 nanotubes by anodization of titanium[J]. *Angewandte Chemie International Edition*, 2005, **44**(14): 2100 − 2102. DOI: 10.1002/anie.200462459.

[16] Varghese O K, Gong D W, Paulose M, et al. Crystallization and high-temperature structural stability of titanium oxide nanotube arrays[J]. *Journal of Materials Research*, 2003, **18**(1): 156 − 165. DOI: 10.1557/jmr.2003.0022.

[17] Taveira L V, Macak J M, Sirotna K, et al. Voltage oscillations and morphology during the galvanostatic formation of self-organized TiO_2 nanotubes[J]. *Journal of the Electrochemical Society*, 2006, **153**(4): B137 − B143. DOI:

10.1149/1.2172566.
[18] Katuri K P, Rengaraj S, Kavanagh P, et al. Charge transport throughGeobacter sulfurreducens biofilms grown on graphite rods[J]. *Langmuir*, 2012, **28**(20): 7904 - 7913. DOI: 10.1021/la2047036.
[19] Hou J X, Liu Z L, Zhang P Y. A new method for fabrication of graphene/polyaniline nanocomplex modified microbial fuel cell anodes[J]. *Journal of Power Sources*, 2013, **224**: 139 - 144. DOI: 10.1016/j.jpowsour.2012.09.091.
[20] Wang H Y, Wang G M, Ling Y C, et al. High power density microbial fuel cell with flexible 3D graphene-nickel foam as anode[J]. *Nanoscale*, 2013, **5**(21): 10283 - 10290. DOI: 10.1039/c3nr03487a.
[21] Katuri K P, Kavanagh P, Rengaraj S, et al. Geobacter sulfurreducens biofilms developed under different growth conditions on glassy carbon electrodes: insights using cyclic voltammetry[J]. *Chemical Communications*, 2010, **46**(26): 4758 - 4760. DOI: 10.1039/c003342a.
[22] Okamoto A, Nakamura R, Nealson K H, et al. Bound-flavin model suggests similar electron-transfer mechanisms in Shewanella and Geobacter[J]. *ChemElectroChem*, 2014, **1**(11): 1808 - 1812. DOI: 10.1002/celc.201402151.
[23] Okamoto A, Hashimoto K, Nealson K H, et al. Rate enhancement of bacterial extracellular electron transport involves bound flavin semiquinones[J]. *Proceedings of the National Academy of Sciences*, 2013, **110**(19): 7856 - 7861. DOI: 10.1073/pnas.1220823110.
[24] Jensen H M, Teravest M A, Kokish M G, et al. CymA and exogenous flavins improve extracellular electron transfer and couple it to cell growth in Mtr-expressing Escherichia coli[J]. *ACS Synthetic Biology*, 2016, **5**(7): 679 - 688. DOI: 10.1021/acssynbio.5b00279.
[25] Hou Y P, Zhang R D, Yu Z B, et al. Accelerated azo dye degradation and concurrent hydrogen production in the single-chamber photocatalytic microbial electrolysis cell[J]. *Bioresource Technology*, 2017, **224**: 63 - 68. DOI: 10.1016/j.biortech.2016.10.069.
[26] Liu Y N, Zhang F, Li J, et al. Exclusive extracellular bioreduction of methyl orange by azo reductase-free geobacter sulfurreducens[J]. *Environmental Science & Technology*, 2017, **51**(15): 8616 - 8623. DOI: 10.1021/acs.est.7b02122.
[27] Fang Z, Cao X, Li X X, et al. Electrode and azo dye decolorization performance in microbial-fuel-cell-coupled constructed wetlands with different electrode size during long-term wastewater treatment[J]. *Bioresource Technology*, 2017, **238**: 450 - 460. DOI: 10.1016/j.biortech.2017.04.075.

二氧化钛纳米管的表面形态对生物电化学系统性能的影响评价

张 田[1] 隆曦孜[1] 曹 羡[2] 李先宁[1]

([1]东南大学能源与环境学院,南京 210096)
([2]Department of Civil and Environmental Engineering, Tohoku University, Sendai 980-8579, Japan)

摘要:为了探究二氧化钛半导体的表面形态和电阻对电流输出的影响,在不同的电解液温度下合成二氧化钛纳米管阵列生物阳极(TNA),从而改变纳米管的长度和表面粗糙度. 结果表明:当阳极氧化温度从 30 ℃升高到 75 ℃时,TNA 的长度从 1.459 μm 增加到 4.183 μm,高温下得到较长纳米管的电阻较大,不利于电子传递至电极;另一方面,较高的温度下制备的纳米管顶端粗糙度明显提高,更大的粗糙度有利于产电菌生物膜的附着. 因此,45 ℃阳极氧化条件下制备的样品输出电流最高. 与 30 ℃阳极氧化条件下制备的 TNA 电极相比,45 ℃的样品平衡了电阻与粗糙度,具有更高的电子传输速率,其电流输出密度和脱色率分别增加了 1.5 倍和 0.8 倍. 因此,适当的 TNA 表面形态能提高电流输出和废水处理方面的潜能.

关键词:生物电化学系统;二氧化钛纳米管阵列;阳极氧化;产电;表面形态
中图分类号:X382